J. Fluid Mech. (1969), *vol.* 39, *part* 1, *pp.* 117–141
Printed in Great Britain

Structural similarity for fully developed turbulence in smooth tubes

By W. R. B. MORRISON
University of Queensland, Brisbane, Australia
AND R. E. KRONAUER
Harvard University, Cambridge, Massachusetts U.S.A.

(Received 23 September 1968)

The structure of fully developed turbulence in smooth circular tubes has been studied in detail in the Reynolds number range between 10,700 and 96,500 (R based on centre velocity and radius). The data was taken as longitudinal and transverse correlations of the longitudinal component of turbulence in narrow frequency bands. By taking Fourier transforms of the correlations, cross-power spectral densities are formed with frequency, ω, and longitudinal or transverse wave-number, k_x or k_z, as the independent variables. In this form the data shows the distribution of turbulence intensity among waves of different size and inclination, and permits an estimate of the phase velocity of the individual waves.

Data taken at radii where the mean velocity profile is logarithmic show that the waves of smaller size (higher $(k_x^2+k_z^2)^{\frac{1}{2}}$) decrease in intensity more rapidly with distance from the wall than the larger waves, and also possess lower phase velocity. This suggests that the waves might constitute a geometrically similar family such that the variation of intensity with wall distance is a unique function with a scale established by $(k_x^2+k_z^2)^{-\frac{1}{2}}$. The hypothesis fits the data very well for waves of small inclination, $\alpha = \tan^{-1}(k_x/k_z)$, and permits a collapse of the intensity data at the several radii into a single 'wave-strength' distribution. The function of intensity with wall distance which effects this collapse has a peak at a wall distance roughly equal to $0{\cdot}6(k_x^2+k_z^2)^{-\frac{1}{2}}$. For waves whose inclination is not small, it would not be expected that the intensity data could collapse in this way since the measured longitudinal component of turbulence represents a combination of two turbulence components when resolved in the wave co-ordinate system.

Although the similarity hypothesis is strictly true only for data taken where the mean velocity profile is logarithmic, a simple correction procedure has been discovered which permits the extension of the similarity concept to the sublayer region as well. This procedure requires only that the observed total turbulence intensity at any station in the sublayer be reduced by a factor which depends solely on the y^+ distance from the wall (i.e. on the distance from the wall, scaled by the viscid parameters of the sublayer). The correction factor is independent of Reynolds number and applies equally to waves of all sizes. In this way, all of

the turbulence waves down to the very smallest of any significance, are found to satisfy slightly modified similarity conditions.

From the data taken at Reynolds numbers between 96,500 and 46,000 wave 'strength' is seen to be distributed more or less uniformly over a range bounded at one extreme by the largest waves which the tube can contain ($k_x^2+k_z^2 \cong (2/a)^2$, where a is the tube radius) and at the other extreme by the smallest waves which can be sustained against the dissipative action of viscosity ($k_x^2+k_z^2 \cong (0{\cdot}04\nu/U_\tau)^2$, where U_τ is the shear velocity). As the Reynolds number of the flow is lowered, the spread between the bounds becomes smaller. If the data is projected to a Reynolds number of order 10^3 the bounds coalesce and turbulence should no longer be sustainable.

1. The nature of the data

Steady, fully developed turbulence in a straight smooth circular tube represents one of the simplest cases of shear flow turbulence. The structure of this turbulence, that is, the description of the turbulent velocity field by two-point space–time correlations, is the concern of the paper. The dependent variables are the three velocity components which have six pair combinations. The independent variables are the three space co-ordinates x, y, z (defined in figure 1) and time, t. Assuming that correlations are stationary in the x, z, and t variables, there are then only five arguments for correlation functions: x_1-x_2, z_1-z_2, t_1-z_2, y_1, y_2. A complete description of turbulence structure therefore requires six functions of five arguments each. Even if such massive data were available, it would be necessary somehow to extract essential simple features before it could be understood and made use of.

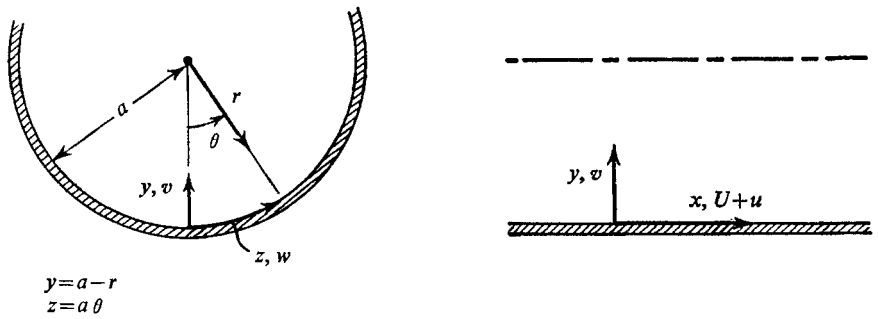

FIGURE 1. Co-ordinates and velocity components.

The data reported here deals only with u_1u_2 correlations (velocities defined in figure 1). The arguments x_1-x_2, z_1-z_2, and t_1-t_2 are explored extensively at different y, but no correlations are taken where y_1 is different from y_2.

Correlations taken in a 'stationary'argument such as x_1-x_2 or t_1-t_2 may be Fourier transformed in that argument to yield power spectral densities with the corresponding transform arguments being k_x and ω. Since the variable z is closed, correlations must be periodic in z_1-z_2 and in a strict sense a Fourier transform cannot be taken, but rather a Fourier series expansion should be used.

Practically, significant correlations are restricted to a small arc (about one radian) so that a Fourier transform in $z_1 - z_2$ can be effected simply by requiring the correlation to vanish at all large arguments. The corresponding transform argument is k_z. For the y co-ordinate, the lack of stationarity prohibits Fourier transformation, although an eigenfunction expansion of any correlation can be effected by the solution of an integral equation with the correlation as the kernel function (Lumley 1967). Since no data was taken with $y_1 \neq y_2$ these manipulations are not possible here, but the interpretation given below of the existing data shows that much insight into turbulence structure can be gained without resort to this complexity.

Correlation functions and power spectral densities are conjugate ways of expressing the same data. The data reported here was taken in mixed form; that is, frequency filters were used so that the transform in the time variable already existed, but spatial co-ordinates were the other natural arguments. For a consistent treatment it was necessary either to invert the time transform or perform the spatial transforms. The latter course was selected because of ample evidence given by visualization techniques (Runstadler, Kline & Reynolds 1963) that pseudo-periodic structures existed, and the description of such structures is more concise in the transform variables. Further justification of this course will be given below.

Consider briefly the kind of data generated at a fixed distance from the surface, y. The power spectral density is a function of the three variables k_x, k_z and ω. It is real and is unchanged if the signs of all three arguments are reversed. Therefore we may ignore the negative régime of any one of the arguments and so adopt the convention that $\omega \geqslant 0$. Further, since the time average flow is free of swirl the correlations must be symmetric in $z_1 - z_2$ and the power spectral density must be symmetric in k_z. Therefore only the régime $k_z \geqslant 0$ need be described. Finally, with $\omega \geqslant 0$ the régime $k_x > 0$ corresponds to waves with an upstream phase velocity. Previous investigations have shown that negligible turbulence energy exists in such waves† so that the region $k_x > 0$ need not be considered. *For convenience the sign of k_x will be reversed throughout this paper.* Thus, when the power spectral density in the region $\omega > 0$, $k_x > 0$, $k_z > 0$ is described, the reader should understand that the waves are in fact propagating downstream and that the power is in fact divided equally between waves of positive and negative k_z.

To generate the three-dimensional power spectral density defined above it is necessary to take a series of correlations in narrow frequency bands and vary the spacings $x_1 - x_2$ and $z_1 - z_2$ jointly. The investigation here was less ambitious: $x_1 - x_2$ was kept at zero while $z_1 - z_2$ was varied, and vice versa. When the transforms of the $z_1 - z_2$ correlations (with $x_1 - x_2 = 0$) are taken, the resulting two-

† For example, the data of Favre, Gaviglio & Dumas (1958) show that a local space correlation at zero delay has a characteristic scale which is an order of magnitude smaller than the characteristic scale when the optimum time shift is used. This demonstrates the strong anisotropy of the Δx, Δt correlation and corresponds to a dominant concentration of power in disturbances propagating with the stream. The surface pressure data of Willmarth & Wooldridge (1962) show even more clearly the absence of any significant upstream propagation.

dimensional power spectral density $P(\omega, k_z)$ is the integration in k_x of the full three-dimensional $P(\omega, k_x, k_z)$. This can be thought of as the integrated 'projection' of $P(\omega, k_x, k_z)$ on the $k_x = 0$ plane (figure 2). Similarly, the transforms of the $x_1 - x_2$ correlations (taken with $z_1 - z_2 = 0$) give the integrated 'projection' of $P(\omega, k_x, k_z)$ on the $k_z = 0$ plane.

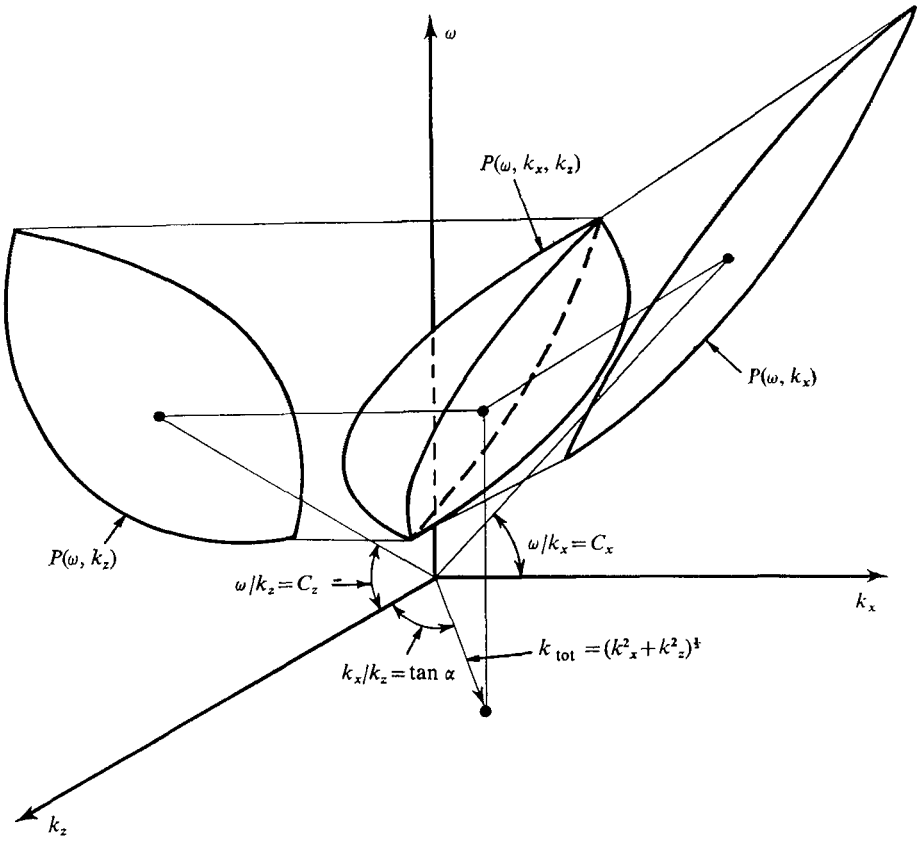

FIGURE 2. Schematic of power distribution in wave-number frequency space.

Fourier transforms of correlation functions give power spectral densities which have the interpretation of power contained within an element of unit width in the frequency or wave-number co-ordinate. Even if the total power is normalized to unity (as is done here) the spectral density has the dimensions of inverse frequency and wave-number. Turbulence in tube flow covers a range of frequency and wave-number on the order of 1000:1, so that a two-dimensional $P(\omega, k_z)$ or $P(\omega, k_x)$ will cover a range of 10^6:1, while $P(\omega, k_x, k_z)$ will cover a range of 10^9:1. Just as logarithmic scales are very useful for the display of the ω, k_x and k_z co-ordinates, so it is convenient to introduce other spectrum functions

$$\mathscr{P}(\omega, k_z) = \omega k_z P(\omega, k_z), \tag{1a}$$

$$\mathscr{P}(\omega, k_x) = \omega k_x P(w, k_x), \tag{1b}$$

$$\mathscr{P}(\omega, k_x, k_z) = \omega k_z k_z P(\omega, k_x, k_z), \tag{1c}$$

which offer several advantages:

(1) they are non-dimensional and the range of interest is about one order of magnitude.

(2) They represent the power in a frequency wave-number region proportional in size to the location of the region. This permits *direct* comparison of the relative power in bands with identical ratios between the upper and lower band limits, i.e. over the same absolute increment on the logarithmic scale.

(3) They are complementary to the logarithmic co-ordinate display since total power is the simple integral of these spectrum functions in the log co-ordinates.

All of the results given in this paper will use these spectrum functions and log co-ordinates.

It has long been known (Laufer 1953) that tube flow turbulence is characterized by a thin layer near the surface where viscosity plays an important role, while in the bulk of the flow (where the mean velocity profile is logarithmic) the phenomena are essentially inviscid. Corresponding to these two régimes the non-dimensionalization of variables is either of the Reynolds or Strouhal variety and neither one will collapse the data throughout the entire field. In this paper an arbitrary choice of Reynolds scaling is made. Thus, with U_τ as the customary shear velocity, the non-dimensional variables are:

$$\left.\begin{aligned} y^+ &= yU_\tau/\nu, \quad k_x^+ = k_x\nu/U_\tau, \\ \omega^+ &= \omega\nu/U_\tau^2, \quad k_z^+ = k_z\nu/U_\tau. \end{aligned}\right\} \tag{2}$$

As mentioned above, two- and three-dimensional power spectral densities are given in normalized form:

$$\left.\begin{aligned} 1 &= \iiint_0^\infty P(\omega^+, k_x^+, k_z^+)\, d\omega^+ dk_x^+ dk_z^+ \\ &= \iiint_{-\infty}^\infty \mathscr{P}(\omega^+, k_x^+, k_z^+)\, d(\ln\omega^+)\, d(\ln k_x^+)\, d(\ln k_z^+), \\ 1 &= \iint_0^\infty P(\omega^+, k_x^+)\, d\omega^+ dk_x^+ = \iint_{-\infty}^\infty \mathscr{P}(\omega^+, k_x^+)\, d(\ln\omega^+)\, d(\ln k_x^+), \\ 1 &= \iint_0^\infty P(\omega^+, k_z^+)\, d\omega^+ dk_z^+ = \iint_{-\infty}^\infty \mathscr{P}(\omega^+, k_z^+)\, d(\ln\omega^+)\, d(\ln k_z^+). \end{aligned}\right\} \tag{3}$$

To find absolute spectral levels at any specified distance from the surface it is necessary to multiply these normalized functions by the total turbulence intensity u^2 at the y^+. The non-dimensionalized form of the intensity is

$$I(y^+) = \overline{u^2}(y^+)/U_\tau^2. \tag{4}$$

All of the data reported here were obtained by hot-wire anemometers in air in a 5·25 in. diameter tube. Six Reynolds numbers (based on centre-line velocity and the tube radius) in the range 10,700–96,500 are represented, corresponding to a range of shear velocities of 0·45–2·80 ft./sec. The details of the experimental technique and reduction of the data are given by Morrison (1969). Confirmation that the data is consistent in its grossest details with other investigations is

afforded by the mean velocity profile (figure 3) and the intensity distribution (figure 4(*a*) and 4(*b*)).

Figures 5(*a*) and 5(*b*) show a sample of the data in the form in which it is generated. These are correlations (transverse in this case) in narrow frequency bands. The scatter seen in these figures is characteristic of the entire body of data. By taking the Fourier transforms of the correlations of figures 5(*a*) and 5(*b*) and then multiplying by the measured frequency spectral density shown in

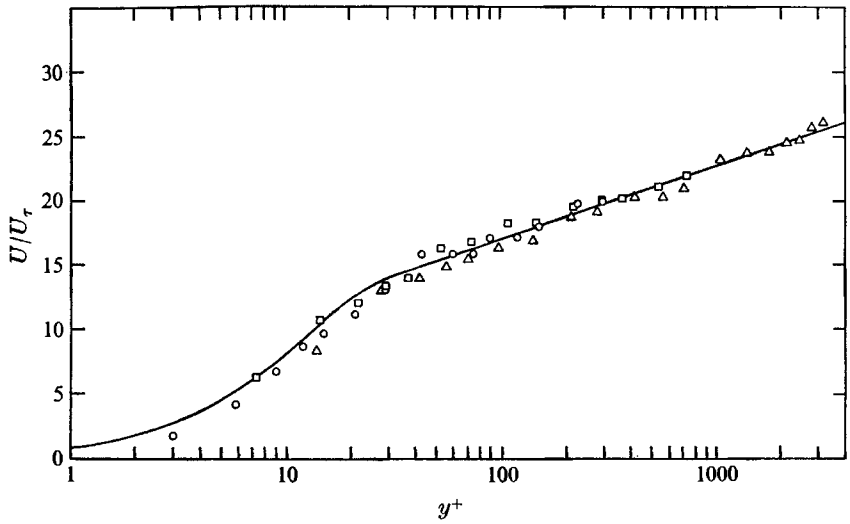

FIGURE 3. Comparison of mean velocity. Data taken by hot wire. Reynolds number: ○, 17,000; □, 46,500; △, 96,500; ———, universal velocity profile.

figure 6, the two-dimensional spectrum function of figure 7(*a*) is generated. In a similar way all of the figures 7(*a*)–7(*r*) are formed and these comprise the body of data to be studied here. The marks on the inside edge of the ω^+ scale in these figures indicate the frequencies at which transverse or longitudinal correlations were actually taken in each case. Table 1 lists the flow conditions corresponding to the 18 parts of figure 7 and in addition lists 5 other $\mathscr{P}$ figures which are reported by Morrison (1969) but which have been omitted here.

Correlations and their transforms (spectra) are, of course, entirely complementary and no information exists in one which is not present in the other. This is not to say that the two forms of presentation lead to equally simple interpretation. It was noted above that the data of Runstadler *et al.* (1963) suggested that a natural wavelike structure exists in boundary layers. Also the linearized perturbation form of the Navier–Stokes equations in the presence of a mean shear field exhibit vorticity wave solutions (see, for example, Landahl 1967). Finally, figures 7(*o*) and 7(*q*) show turbulence disturbances to propagate at speeds significantly different from local flow speed and give evidence of wave structure with significant extent in the direction of the mean velocity gradient. These then constitute reasons for expecting special results from a spectral treatment of the data. One such result is a geometric similarity law which is developed

in the next section. Before proceeding to this development is is relevant to observe that the mathematical statement of geometrical similarity is contained in equation (11) which essentially represents the factorization of a spectrum function into a product. This means that if the data analysis had been performed on correlations rather than spectra we would have been seeking a decomposition

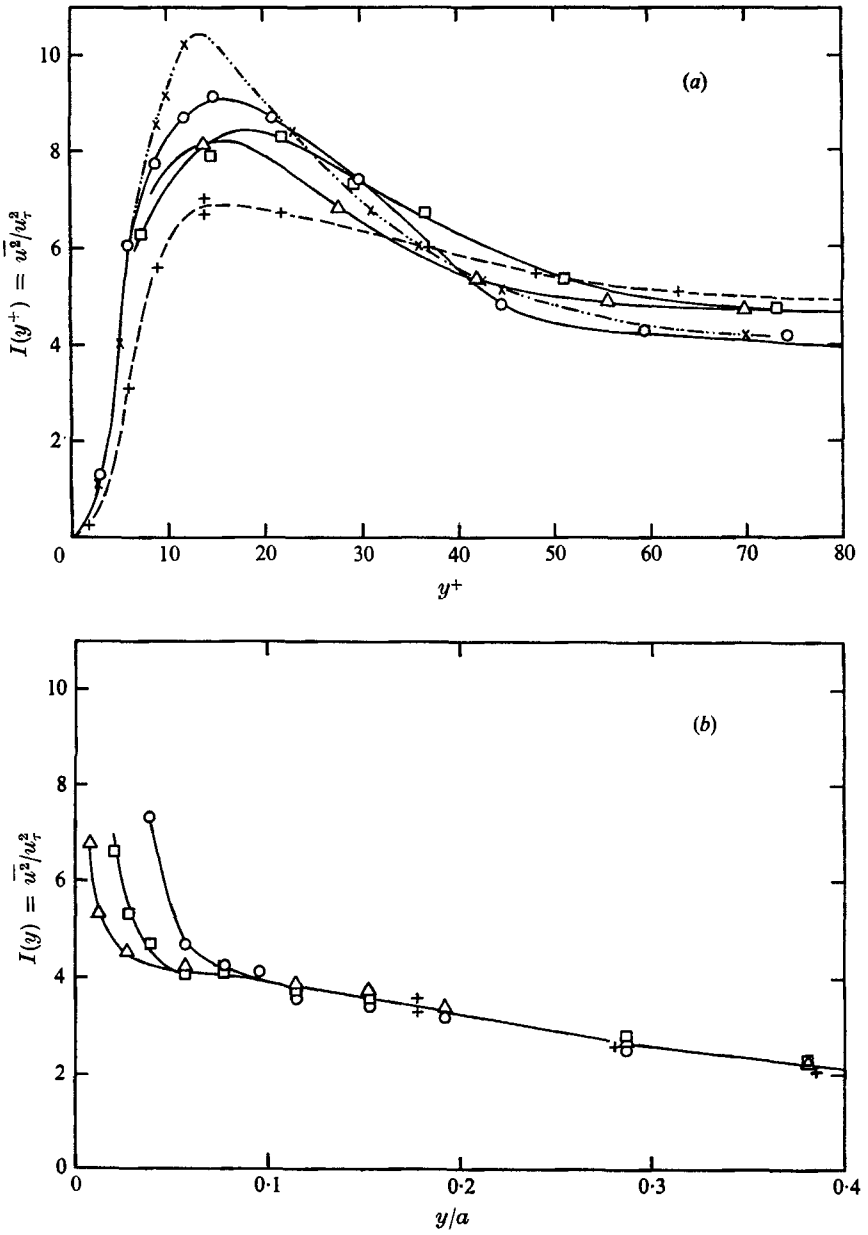

FIGURE 4. Turbulence intensity. (*a*) Reynolds number: ○, 17,000; □, 46,500; △, 96,500; +, 250,000, Laufer (1953); ×, 15,200, Clark (1968). (*b*) Reynolds number: ○, 17,000; □, 46,500; △, 96,500; +, 250,000, Laufer (1963).

of the raw data into a convolution of two unknown functions. The possibility of such a decomposition representing the data would probably not even have occurred to us.

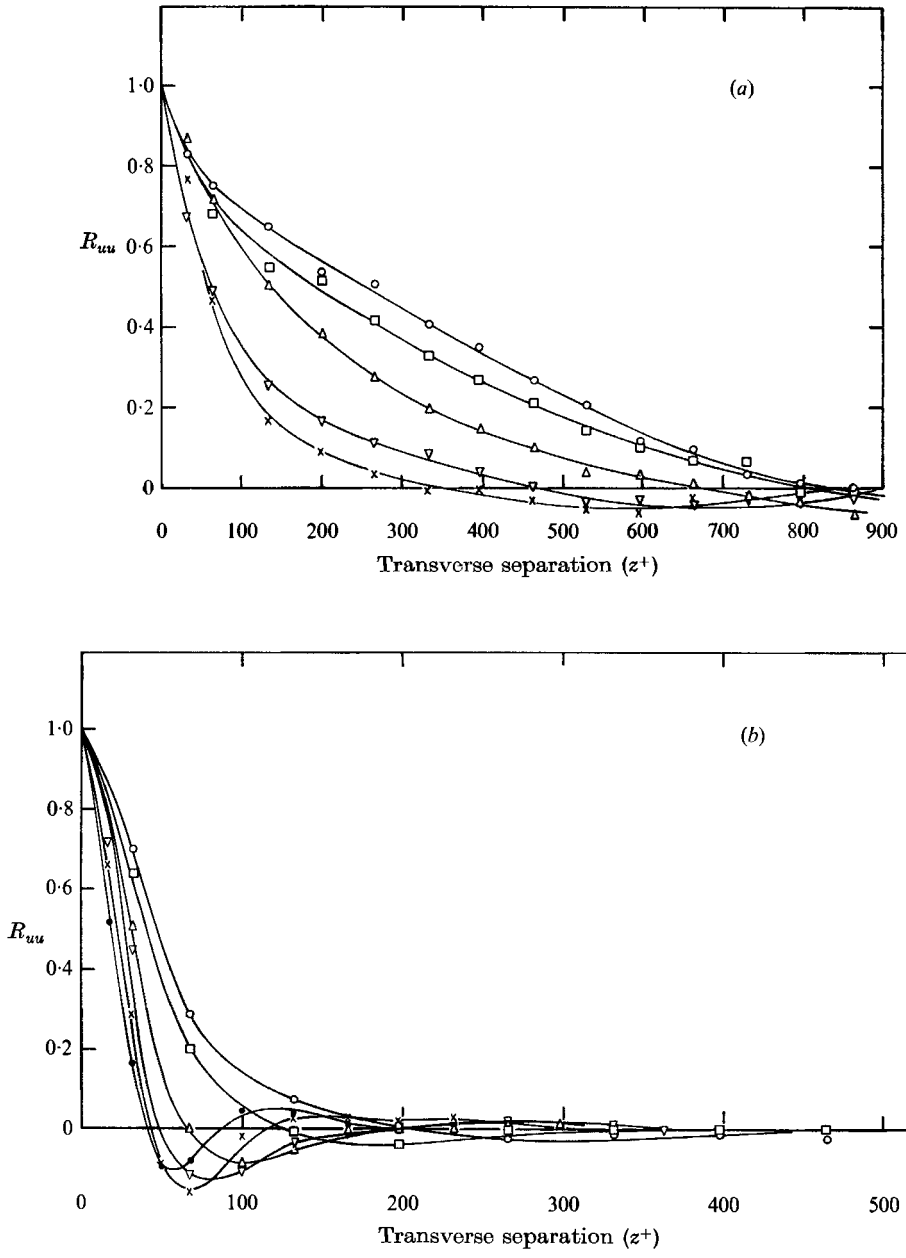

FIGURE 5. *uu* correlation in frequency bands with transverse separation $y^+ = 7.3$, $U_\tau = 1{\cdot}50$. (*a*) ω^+: ○, 0·00170; □, 0·0036; △, 0·0072; ▽, 0·0145; ×, 0·0184. (*b*) ω^+: ○, 0·029; □, 0·041; △, 0·058; ▽, 0·097; ×, 0·194; ●, 0·33.

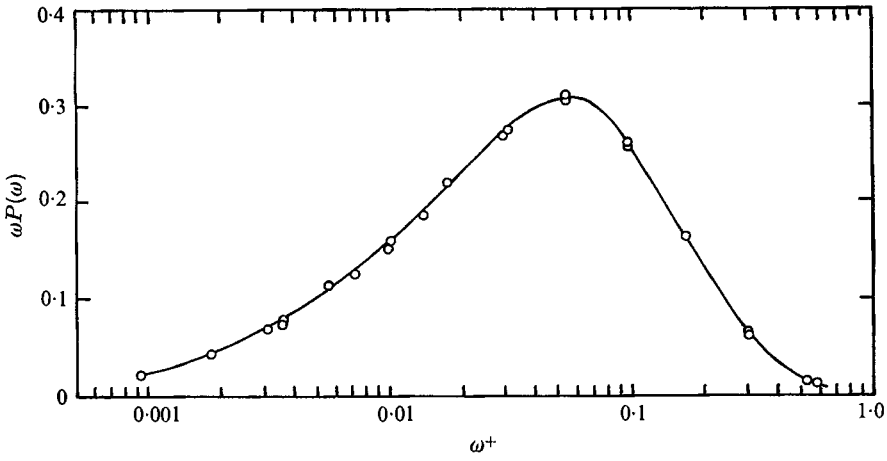

FIGURE 6. Normalized frequency spectrum. $y^+ = 7{\cdot}3$, $U_\tau = 1{\cdot}50$.

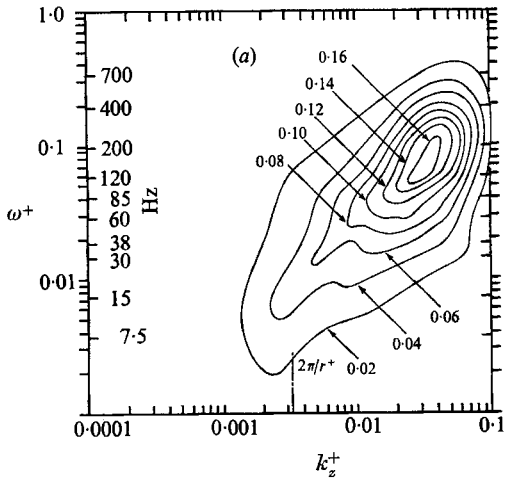

FIGURE 7(*a*). $\mathscr{P}(\omega^+, k_z^+)$, $y^+ = 7{\cdot}3$, $U_\tau = 1{\cdot}50$.

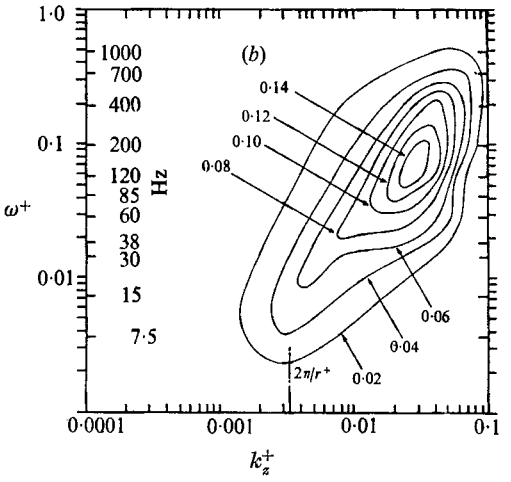

FIGURE 7(*b*). $\mathscr{P}(\omega^+, k_z^+)$, $y^+ = 14{\cdot}6$, $U_\tau = 1{\cdot}50$.

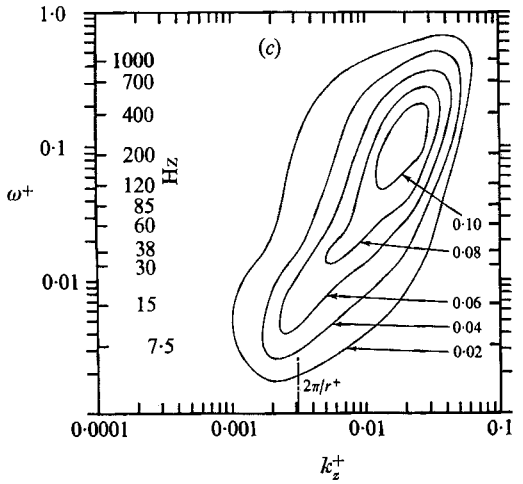

FIGURE 7(*c*). $\mathscr{P}(\omega^+, k_z^+)$, $y^+ = 3{\cdot}80$, $U_\tau = 1{\cdot}50$.

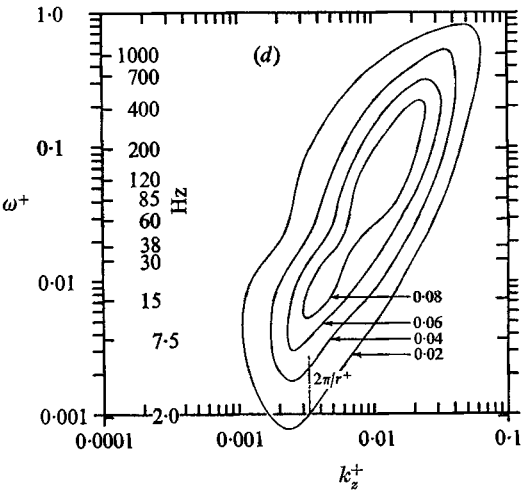

FIGURE 7(*d*). $\mathscr{P}(\omega^+, k_z^+)$, $y^+ = 73{\cdot}0$, $U_\tau = 1{\cdot}50$

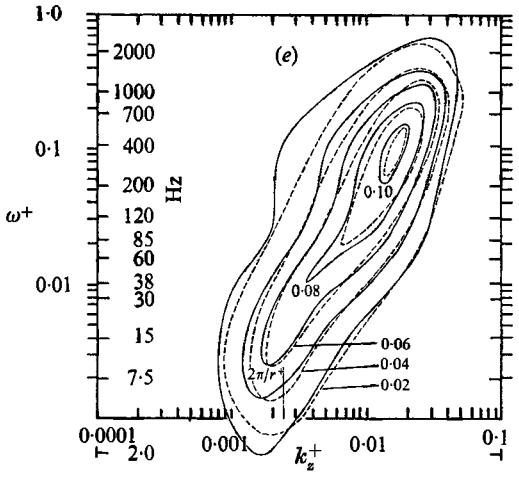

FIGURE 7(e). $\mathscr{P}(\omega^+, k_z^+)$, $y^+ = 49{\cdot}0$, $U_\tau = 2{\cdot}00$.

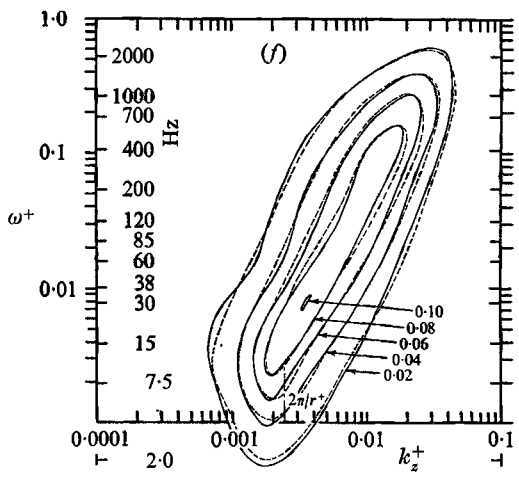

FIGURE 7(f). $\mathscr{P}(\omega^+, k_z^+)$, $y^+ = 99{\cdot}0$, $U_\tau = 2{\cdot}00$.

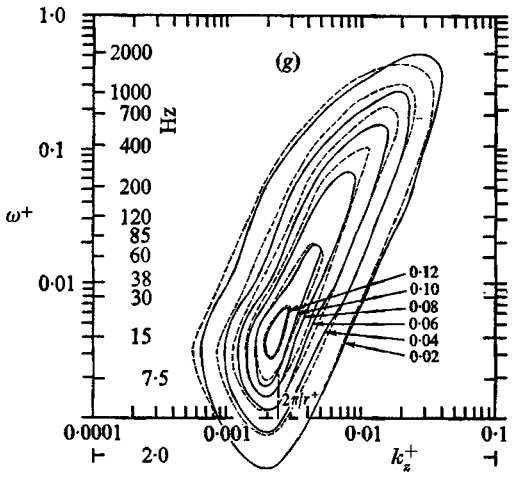

FIGURE 7(g). $\mathscr{P}(\omega^+, k_z^+)$, $y^+ = 198$, $U_\tau = 2{\cdot}00$.

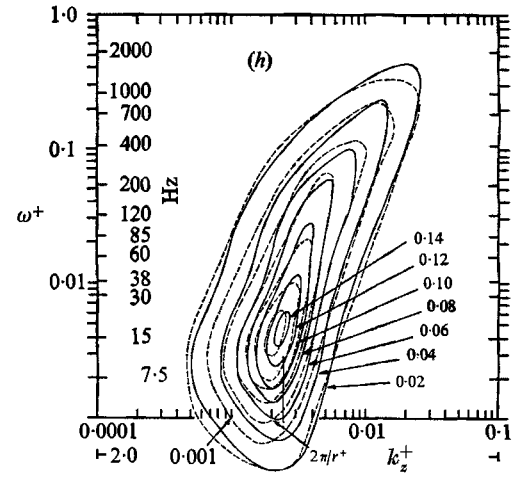

FIGURE 7(h). $\mathscr{P}(\omega^+, k_z^+)$, $y^+ = 395$, $U_\tau = 2{\cdot}00$.

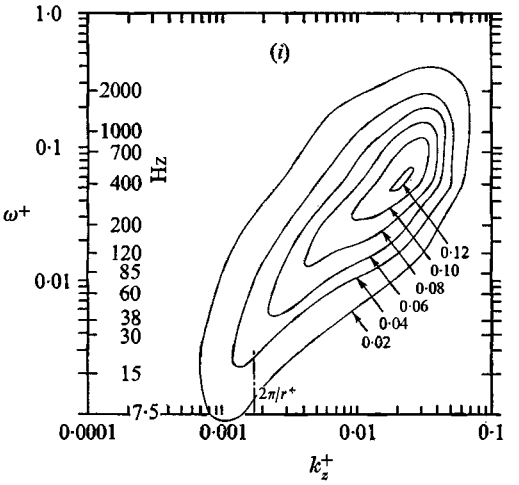

FIGURE 7(i). $\mathscr{P}(\omega^+, k_z^+)$, $y^+ = 13{\cdot}9$, $U_\tau = 2{\cdot}80$.

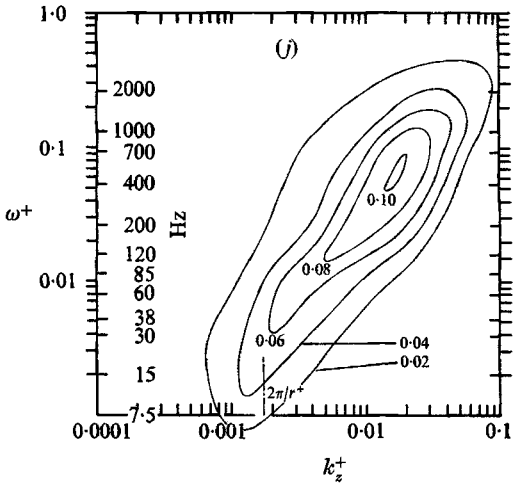

FIGURE 7(j). $\mathscr{P}(\omega^+, k_z^+)$, $y^+ = 27{\cdot}8$, $U_\tau = 2{\cdot}80$.

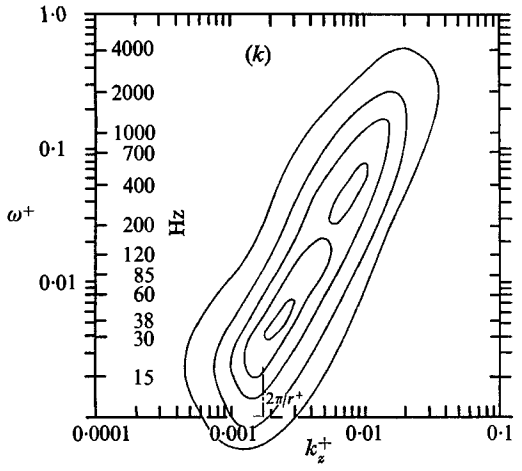

FIGURE 7(*k*). $\mathscr{P}(\omega^+, k_z^+)$, $y^+ = 139$, $U_\tau = 2{\cdot}80$.

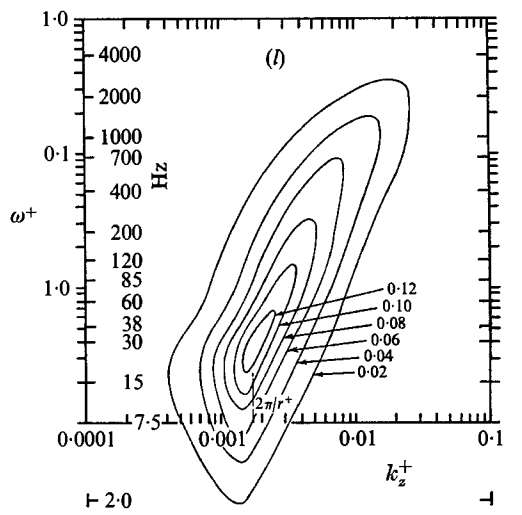

FIGURE 7(*l*). $\mathscr{P}(\omega^+, k_z^+)$, $y^+ = 278$, $U_\tau = 2{\cdot}80$.

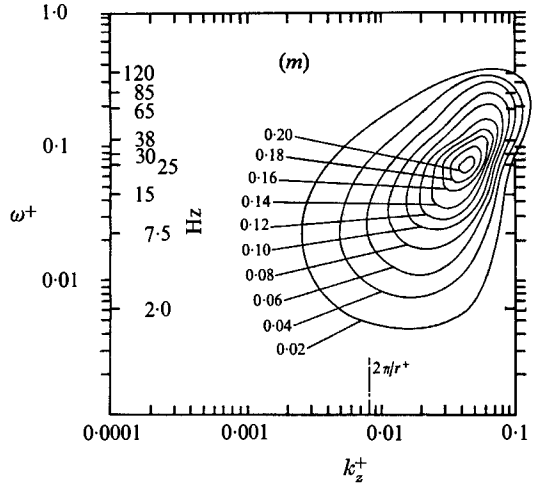

FIGURE 7(*m*). $\mathscr{P}(\omega^+, k_z^+)$, $y^+ = 3{\cdot}0$, $U_\tau = 0{\cdot}60$.

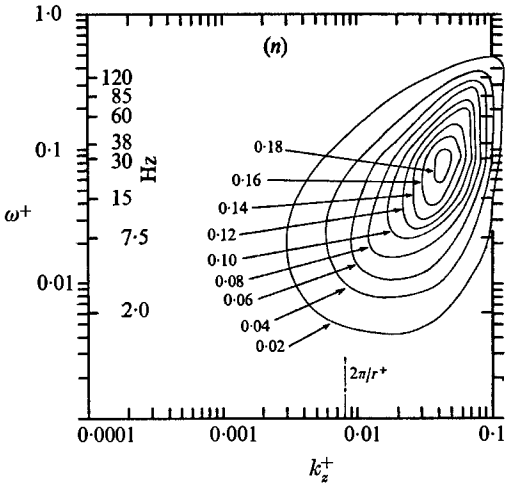

FIGURE 7(*n*). $\mathscr{P}(\omega^+, k_z^+)$, $y^+ = 5{\cdot}9$, $U_\tau = 0{\cdot}60$.

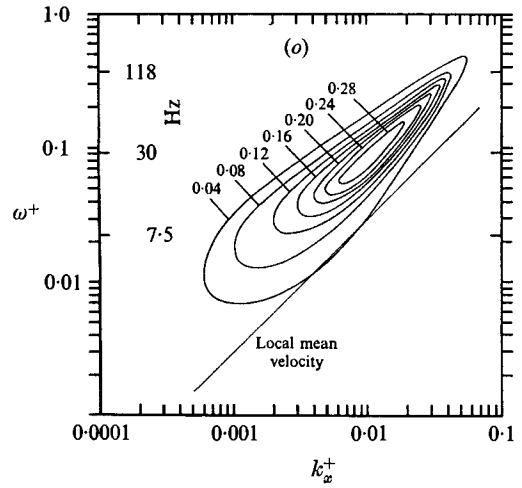

FIGURE 7(*o*). $\mathscr{P}(\omega^+, k_x^+)$, $y^+ = 3{\cdot}0$, $U_\tau = 0{\cdot}60$.

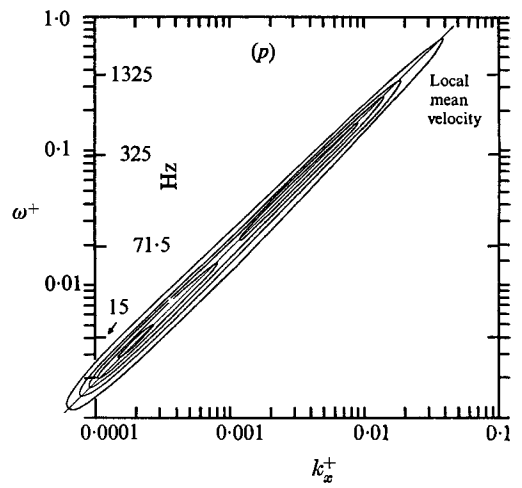

FIGURE 7(*p*). $\mathscr{P}(\omega^+, k_x^+)$, $y^+ = 198$, $U_\tau = 2{\cdot}00$.

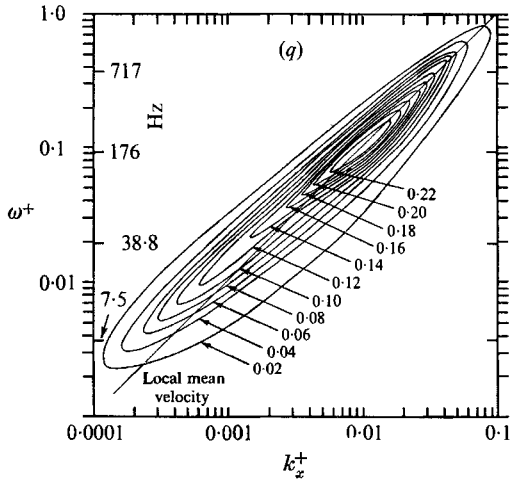

FIGURE 7(q). $\mathscr{P}(\omega^+, k_x^+)$, $y^+ = 14{\cdot}6$, $U_\tau = 1{\cdot}50$.

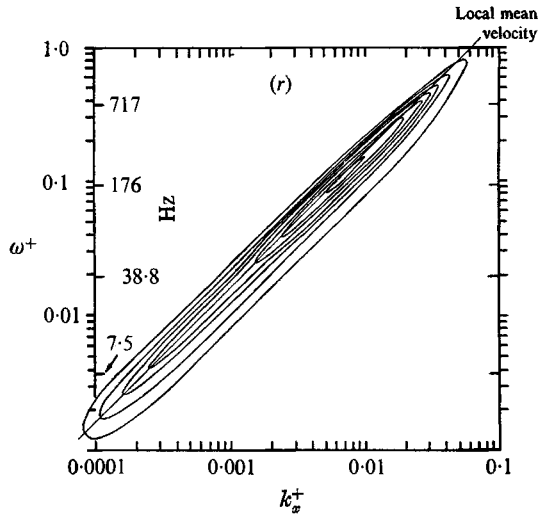

FIGURE 7(r). $\mathscr{P}(\omega^+, k_x^+)$, $y^+ = 73{\cdot}0$, $U_\tau = 1{\cdot}50$.

Figure	U_τ (ft./sec)	$R_1 = U_\tau a/\nu$	y (in.)	y/a	y^+	$I(y^+)$
			$\mathscr{P}(\omega^+, k_z^+)$			
*	0·45	10,700	0·007	0·0026	1·6	0·25
7(*m*)	0·60	17,000	0·010	0·0038	3·0	1·3
7(*n*)			0·020	0·0076	5·9	6·0
*	0·80	24,000	0·050	0·019	20·0	8·4
7(*a*)	1·50	45,600	0·010	0·0038	7·3	6·2
7(*b*)			0·020	0·0076	14·6	7·8
7(*c*)			0·050	0·019	38·0	6·7
7(*d*)			0·100	0·038	73·0	4·8
7(*e*)	2·00	65,300	0·050	0·019	49·0	5·6
7(*f*)			0·100	0·038	99·0	4·6
7(*g*)			0·200	0·076	198	4·3
7(*h*)			0·400	0·152	395	3·7
7(*i*)	2·80	96,500	0·010	0·0038	13·9	8·1
7(*j*)			0·020	0·0076	27·8	6·8
7(*k*)			0·100	0·038	139	4·5
7(*l*)			0·200	0·076	278	4·2
			$\mathscr{P}(\omega^+, k_x^+)$			
*	0·45	10,700	0·007	0·0026	1·6	0·25
7(*o*)	0·60	17,000	0·010	0·0038	3·0	1·3
*			0·020	0·0076	5·9	6·0
*	0·80	24,000	0·050	0·019	20·0	8·4
7(*q*)	1·50	46,500	0·020	0·0076	14·6	7·8
7(*r*)			0·100	0·038	73·0	4·8
7(*p*)	2·00	65,300	0·200	0·076	198	4·3

* May be found in Morrison (1969).

TABLE 1.

2. Reduction of the data

The primary purpose of this paper is to show that the data shown in figures 7 (*a*) to 7 (*r*) (representing over 4000 correlation data points) can be efficiently compressed in a logical manner which, at the same time, gives a simple physical meaning to the result. Before doing this it is important that the interpretation of wave geometry be clear. A point in ω^+, k_x^+, k_z^+ wave space represents a wave with total wave-number

$$k_{\text{tot}}^+ = (k_x^{+2} + k_z^{+2})^{\frac{1}{2}}, \tag{5}$$

with lines of constant phase inclined to the x axis (tube axis) at the angle

$$\alpha = \tan^{-1}(k_x^+/k_z^+), \tag{6}$$

when projected radially outward to the tube surface. Such a wave exhibits a streamwise phase velocity

$$C^+ = \omega^+/k_x^+ = C_x/U_\tau, \tag{7}$$

and a circumferential phase velocity (projected on the tube surface) of

$$C_z^+ = \omega^+/k_z^+ = C_z/U_\tau. \tag{8}$$

These properties are referred to in figure 2 and in the wave schematic diagram, figure 8. Because of the symmetrical distribution of wave power in k_z, right-handed and left-handed helical waves are equally strong. In the diagrams of figure 7, loci of constant phase velocity have unit slope.

There are two general features of the spectrum functions to be observed. First, for $\mathscr{P}(\omega^+, k_x^+)$ data taken in the log layer, the 'ridge' of the spectral distribution corresponds to C_x between about $14U_\tau$ and $22U_\tau$. For the data taken in the sublayer the C_x at the spectral peak drops as low as about $8U_\tau$. Because of the limited total range of C_x^+, for almost all of the data it is possible to make the rough correspondence, $\omega^+ \cong 15k_x^+$. In this way the plots of $\mathscr{P}(\omega^+, k_z^+)$ may be viewed approximately as $\mathscr{P}(k_x^+, k_z^+)$ with a shift of the vertical scale upward by a factor of 15. That is, the $\mathscr{P}(\omega^+, k_z^+)$ roughly represents the distribution of power among waves of various sizes and inclinations. (A locus of constant inclination, α, has then approximately a unit slope in these plots.)

Following upon this fact, the next general feature to be observed from the $\mathscr{P}(\omega^+, k_z^+)$ is that by far the largest amount of power is found in waves of relatively small inclination, α. For the smallest waves, sublayer data shows the dominant α to be about $\frac{1}{4}$ radian while for the largest waves the log layer data places α at about $\frac{1}{10}$ radian. These are waves highly elongated in the x direction, a fact roughly indicated by the early data of Grant (1958) and Favre *et al.* (1958) for the longitudinal turbulence component.

Now we shall try to compress the $\mathscr{P}(\omega^+, k_z^+)$ data for stations in the log layer ($y^+ > 70$) for the several Reynolds numbers. The clue for the procedure is best seen from a comparison of figures 7 (*e*) and 7 (*h*) ($U_\tau = 2{\cdot}0$). Here it is very apparent that in going from $y^+ = 49$ to $y^+ = 395$ there is a strong shift of power away from the high k_z^+. That is, the small waves are relatively weaker at the larger distance from the wall. It is on the basis of this evidence that we make the key hypothesis of this work. If a wave with a small dimension projected on the tube surface,

λ^+_{tot}, has a small radial extent, y^+, while a large wave has a large radial extent, it is possible that waves of all sizes may be geometrically similar. By this we mean that each of the velocity components of the wave ($\hat{u}$, v and $\hat{w}$ as defined in figure 8) would be a unique function of y^+/λ^+_{tot} independent of the size or inclination of the wave and differing only in strength from wave to wave.† In particular this would require the intensity of each velocity component to be a unique function of $k^+_{tot}y^+$ (note $k^+_{tot} = 2\pi/\lambda^+_{tot}$).

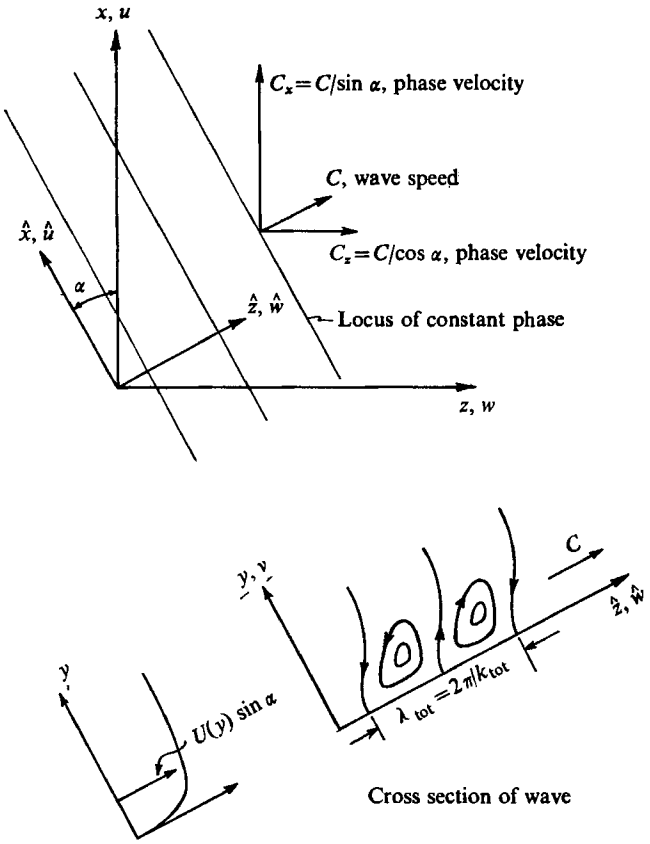

FIGURE 8. Wave schematic diagram.

How may this hypothesis be tested? The available data describe the spectral power in u, which is actually a combination of $\hat{u}$ and $\hat{w}$,

$$u = \hat{u}\cos\alpha + \hat{w}\sin\alpha. \tag{9}$$

Therefore it is a mixture of $\hat{u}$ spectra and $\hat{w}$ spectra and their cross-spectral density as well.‡ If we wish to separate out the $\hat{u}$ or $\hat{w}$, it is necessary to select either

† Some of the analytic consequences of geometric similarity are discussed in the appendix.

‡ For a precise discussion of this point see the appendix.

small α or large α data. The choice is obviously small α. Next it is necessary to form the absolute spectral level at each y^+ by taking the product

$$\tilde{\mathscr{P}}(\omega^+, k_z^+, y^+) = I(y^+)\,\mathscr{P}(\omega^+, k_z^+, y^+). \tag{10}$$

Following this we choose a variety of representative points (ω^+, k_z^+) throughout the data field, but corresponding to small α (i.e. $\omega^+/k_z^+ < 4$). With α small we also have $k_{\text{tot}}^+ \cong k_z^+$. We now regard y^+, or more precisely, $k_{\text{tot}}^+ y^+$, as the relevant independent variable and plot $\hat{\mathscr{P}}$ *vs.* $k_{\text{tot}}^+ y^+$ for each of the chosen points (ω^+, k_z^+). If the similarity hypothesis is valid, it should be possible to find a radial distribution function for intensity, $f(k_{\text{tot}}^+ y^+)$, applicable to all waves, such that all the invididual plots of $\tilde{\mathscr{P}}$ can be represented by the factorization:

$$\tilde{\mathscr{P}}(\omega^+, k_{\text{tot}}^+ y^+) = f(k_{\text{tot}}^+ y^+)\,A(\omega^+, k_z^+). \tag{11}$$

Here $A(\omega^+, k_z^+)$ is a function which we will call the wave strength, which depends on the size and inclination of the particular wave. The data for $U_\tau = 2{\cdot}80$ and $U_\tau = 2{\cdot}0$ do in fact collapse on this basis giving the $f(k_{\text{tot}}^+ y^+)$ shown in figure 9 and the A distributions shown in figures 10 and 11 (actually only the solid portions of the A contours, since these correspond to the small α). Since a product decomposition of the form of (11) is arbitrary to the extent of a scalar multiple of one factor, f has been chosen so that its maximum has a value of unity.

The quality of the collapse of the data can be judged from figures 7 (f) to 7 (h). The dashed contours in these figures represent the $\mathscr{P}$ calculated backward from the A of figure 10 and f of figure 9. In no case do the values given by the calculation differ from the data by more than 15 % of the maximum value of $\mathscr{P}$ in the particular figure, with typical differences less than 7 %.

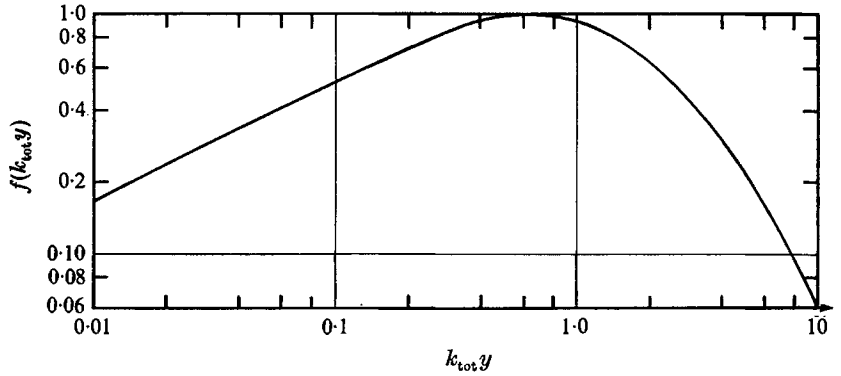

FIGURE 9. Wave intensity function for $\hat{u}$.

3. Extension of the data reduction to low y

If the $\mathscr{P}(\omega^+, k_z^+)$ data for $y^+ = 27{\cdot}8$ and $y^+ = 13{\cdot}9$ with $U_\tau = 2{\cdot}80$ (figures 7 (i) and 7 (j)) are compared with the predictions derived from the A and f just calculated, it happens that the shape of the predicted $\mathscr{P}$ distributions match the data, but their general level is much lower. This suggests that perhaps the similarity concept can be extended to $y^+ < 70$ by the simple expedient of reducing the experimental $I(y^+)$ by a correction factor. This expedient works very

well, and the appropriate correction factor is given in figure 12. Not only does it work for the $U_\tau = 2{\cdot}80$ data, but also for $U_\tau = 2{\cdot}0$ and $U_\tau = 1{\cdot}50$ as well. (Since only one $y^+ > 70$ was available for $U_\tau = 1{\cdot}50$, it could not be treated without the correction. With the correction, the data at $y^+ = 7{\cdot}3$, $14{\cdot}6$ and 38 are used together

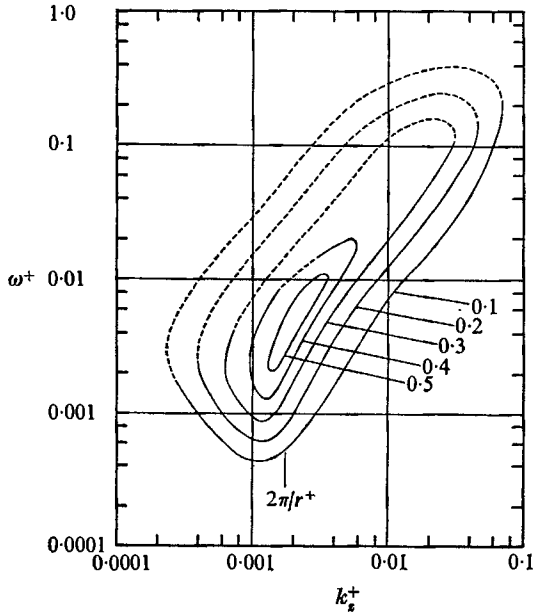

FIGURE 10. Wave strength, A. $U_\tau = 2{\cdot}82$ ft./sec, $R = 96{,}500$.

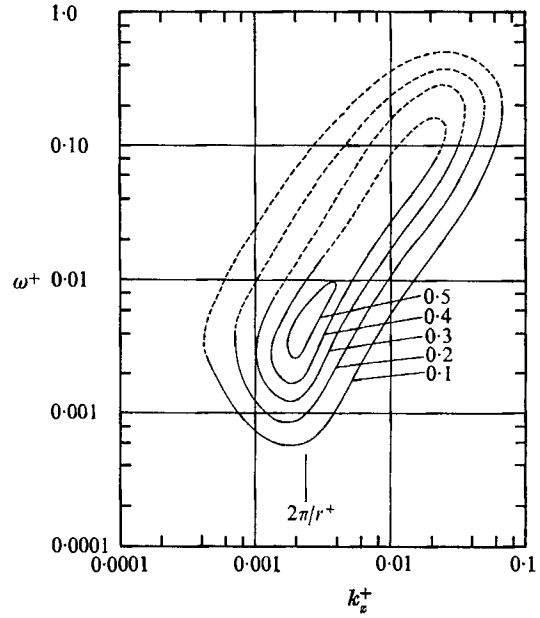

FIGURE 11. Wave strength, A. $U_\tau = 2{\cdot}0$ ft./sec, $R = 65{,}300$.

with $y^+ = 73$.) The resulting A for $U_\tau = 1{\cdot}50$ is seen in figure 13. Some idea of how well this correction works is given by figure 7 (*e*). Here a 17 % reduction of $I(y^+)$ has been used and the 'backward' calculation of $\mathscr{P}$ from A and f is seen to be excellent.

There is a simple mechanism which seems to explain most of the correction used. The similarity hypothesis which proved successful in collapsing the $\hat{u}$ data

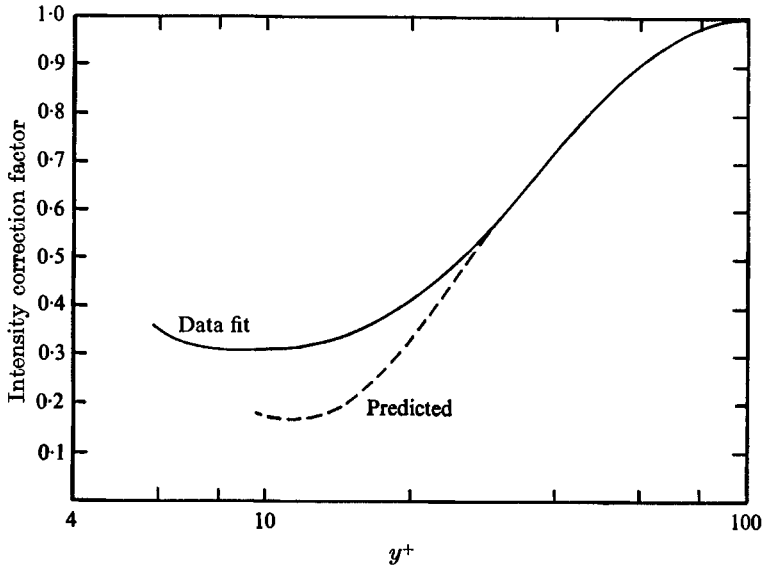

FIGURE 12. Intensity correction factor.

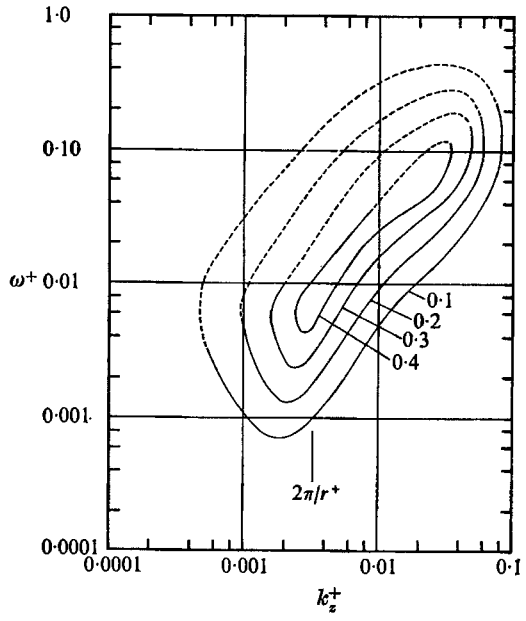

FIGURE 13. Wave strength, A. $U_\tau = 1{\cdot}48$ ft./sec, $R = 46{,}500$.

in the log layer should, of course, apply to all wave velocity components, although with different radial distribution functions. If one writes the linearized Navier–Stokes equations in the wave co-ordinates $\hat{x}$, y, and $\hat{z}$ shown in figure 8 (as in the appendix), the equations containing v and $\hat{w}$ are independent of $\hat{u}$ and may be solved separately. The resulting v may then be used in the equation for $\hat{u}$ where it appears as a 'driving' term multiplying dU/dy. Since the solution for v is only slightly affected by the deviation of the mean velocity profile from logarithmic near the wall (i.e. v retains its similarity properties), the driving term in the $\hat{u}$ equation will increase at low y^+ as dU/dy becomes larger than that which the log function would show, were it to extend that far. The difference produces a local deviation of $\hat{u}$ from log law similarity. Reasoning in this way, a correction to $\hat{u}$ (which is, of course, u for waves of small α) can be estimated as shown in figure 14. From the actual mean velocity profile and the experimentally

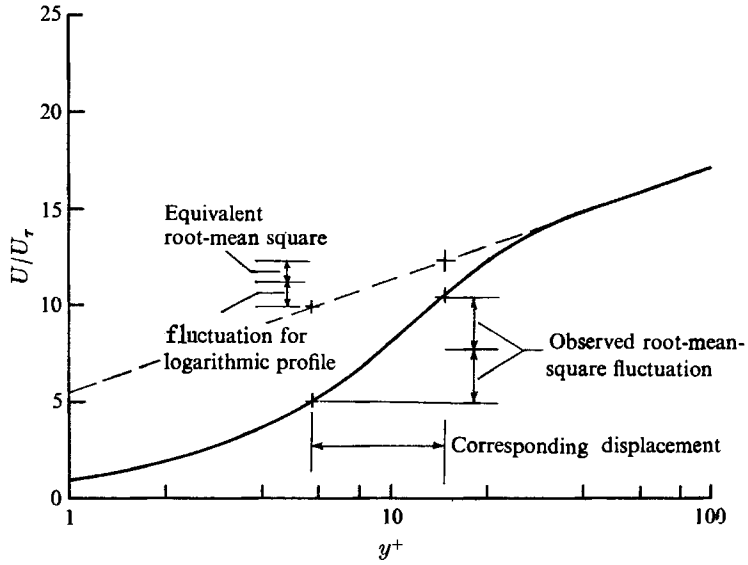

FIGURE 14. Prediction of intensity correction factor.

measured root-mean-square u fluctuation, a representative displacement of fluid normal to the wall is deduced. The displacement is used in turn to obtain an apparent root-mean-square u fluctuation, which would have been found had the log profile persisted to lower y^+. The square of the ratio of the apparent to the true u is the predicted intensity correction factor shown in figure 12. The prediction is excellent down to a y^+ of 25 where, apparently, direct effects of viscosity become important.

In summary, the experience with the intensity correction suggests that while $\hat{u}$ deviates from strict similarity for $y^+ < 70$, v does not deviate from similarity until $y^+ < 25$. Whether or not this interpretation of the data stands up under further detailed measurements, the experimental fact remains that the simple expedient of adjusting intensity works, and works independently of the size and inclination of the individual waves. While the data for the three Reynolds

numbers in question extends only to $y^+ = 7$, the $\mathscr{P}(\omega^+, k_z^+)$ at lower Reynolds number, figures 7(*m*) and 7(*n*) exhibit very small changes of spectral distribution between $y^+ = 10$ and the wall, so it is highly probable that an intensity correction will work right down to $y^+ = 0$.

4. Extension of the data reduction to large α

As long as we are studying only small α, the wave size is determined essentially by k_z^+ and it is never necessary to invoke the approximation $\omega^+ \cong 15 k_x^+$ specifically. The assumption actually used is simply that each point with co-ordinates (ω^+, k_z^+) correspond to *some* (k_x^+, k_z^+) and the *same* (k_x^+, k_z^+) at each y^+. In fact the assumption can be relaxed further, so that k_x^+ is permitted to occupy a small band of values at each ω^+ provided the band is the same at each y^+. However, when considering large α, it is advisable to have the best possible estimate of k_x^+ since it figures importantly in k_{tot}.

Since we already have convincing evidence that turbulence waves are geometrically similar, the similarity property can be used to estimate C_x. The important region for wave interaction with the mean flow is the so-called critical layer (Lin 1955) where the wave speed matches the mean flow speed. For a similar family of waves it is shown in the appendix that height of the critical layer, y_0^+, will scale with λ_{tot}^+, i.e. $k_{\text{tot}}^+ y_0^+ = \text{const}$. To check this point experimentally would require the full three-dimensional power spectral density $P(\omega, k_x, k_z)$ shown in figure 2, and not just the two projections $P(\omega, k_x)$ and $P(\omega, k_z)$ actually available. Interpreting the projected data in the most favourable way (by an analysis too detailed to report here), we conclude that, although there is a considerable spread in the results, $k_{\text{tot}}^+ y_0^+ = 0{\cdot}6$ is a reasonable approximation. Using this, a choice of k_{tot}^+ yields a value of y_0^+ which in turn gives C_x^+ from the mean velocity profile. A second choice, that of ω^+, yields k_x^+ and thence k_z^+. Thus we have a unique implicit relationship between (ω^+, k_z^+) and (k_x^+, k_z^+).

In § 2 we observed that

$$u = \hat{u} \cos\alpha + \hat{w} \sin\alpha. \tag{9}$$

Thus, as α increases, the content of u shifts from $\hat{u}$ to $\hat{w}$. While we certainly expect $\hat{w}$ to be similar for different size waves, it may have an intensity distribution function different from the $f(k_{\text{tot}}^+ y^+)$ which characterizes $\hat{u}$.

If we denote the similarity function for w as g_2, as in the appendix, data for $\tan\alpha > 3$ (where $\hat{u}$ is unimportant) shows that g_2 has a maximum shaped very much like the maximum of f but located at an argument, $k_{\text{tot}}^+ y^+$, nearly 4·5 times as large. Data for intermediate α consistently show similar maxima, the location proceeding smoothly from the location of $f_{\max}$ to the location of $g_{\max}$ as $\tan\alpha$ increases from $\frac{1}{4}$ to 3. This suggests that the function f might be used at all α, provided its argument were modified to be a function of α. Introducing the function $\sigma(\alpha)$ shown in figure 15, which describes the shift of the maximum relative to the original maximum of f, we try the correlation $f(k_{\text{tot}}^+ y^+/\sigma(\alpha))$ for all the α previously omitted. This works very well, in fact, as well as the original f for small α, and has been used to produce the dotted portions of the A contours in

figures 10, 11 and 13. It is our opinion that while the location of maxima and the intensities near maxima are well fitted by this simple scheme, it is unlikely that g_2 far away from maximum will indeed resemble f very closely. Our data here is weak and direct measurements of w (transverse velocity in the tube co-ordinates) are needed.

It is of interest to note that data taken at low y^+ displaying large α is subject to *two* correction procedures. These seem to be applicable concurrently since the data treated in this way collapse with no worse accuracy than the data in general.

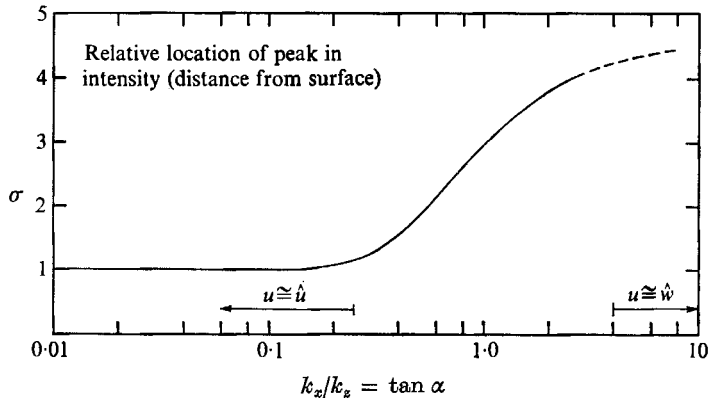

FIGURE 15. Dependence of intensity peak on wave inclination.

5. Comparison of the different Reynolds numbers

The figures 10, 11 and 13 show the wave strength for successively decreasing Reynolds numbers: 96,500, 65,300, and 46,500. Although wave data were taken down to $R = 10{,}700$, at any particular R this does not cover a sufficiently large range of y^+ to permit a reliable calculation of A. However, within the more limited range for which A is given, some distinct trends may be seen.

First, the high k_z^+ end of the figures show a pattern of distribution of strength among the small waves which is substantially independent of Reynolds number to the degree of accuracy of the data. These waves have a characteristic dimension matched to the dimension of the sublayer. Their wavelength is of order $\lambda_{\text{tot}}^+ = 150$ and their C_x is about $9U_\tau$. This latter value places the 'critical layer' of these smallest waves at a $y^+ = 12$. These waves are equally divided between right- and left-hand helical components which exhibit opposite circumferential phase velocity. The combination of these components gives, roughly, a wave structure, 'standing' in the z co-ordinate but travelling in x and t with a wavelength $\lambda_x^+ \cong 500$ and the phase velocity $C_x = 9U_\tau$. It is this standing wave pattern which gives rise to the longitudinal 'streaks' found in the visualization studies of Runstadler *et al.* (1963). The reason these streaks are so clearly visible is that there is no smaller structure in the flow to disrupt their organization.

Considering next the low k_z^+ end of the A distributions, we again observe a strong similarity of shape between the different Reynolds numbers, although the characteristic ω^+ and k_z^+ are lower at the higher U_τ. This is because the viscid

scaling which was adopted is not applicable to the large waves. The appropriate inviscid scaling is:

$$x^* = x/a, \qquad \omega^* = \omega a/U_\tau,$$
$$y^* = y/a, \qquad k_x^* = k_x a,$$
$$z^* = z/a = \Theta, \qquad k_z^* = k_z a.$$

If these variables are introduced, the low k_z end of the A distributions are seen to coincide very well in shape although the magnitude of A for different Reynolds numbers is somewhat different. (The change of variables corresponds to relative translation of the A distributions along a direction with unit slope in the ω^+, k_z^+ co-ordinates, the amount of the translation in either ω^+ or k_z^+ being the ratio of the U_τ for the cases in question.) The largest waves have an inclination α of about $\frac{1}{10}$. Their total wavelength (which is equivalent to transverse wavelength for this small α) is about one radius for the dominant power and about one-half the circumference for the limiting size. The C_x for the dominant waves corresponds quite closely to the mean velocity at $y/a = 0{\cdot}1$.

It has been pointed out (e.g. Bradshaw 1967) that for stations in the log layer and for the central range of wave-numbers the distribution of power among the wave-numbers should scale solely on the basis of the distance to the surface. If we ignore the small variations in convective velocity for waves in this range so that ω^+ can be replaced by a multiple of k_x^+, then the spectrum function appearing on the left side of (11) can be written with the arguments $\tilde{\mathscr{P}}(k_x^+, k_z^+, y^+)$ or, better still, $\tilde{\mathscr{P}}(k_{\text{tot}}^+, \alpha, y^+)$. The implication of the Bradshaw (1967) remark is that these arguments must appear in combination thus: $\tilde{\mathscr{P}}(k_{\text{tot}}^+ y^+, \alpha)$. On the other hand, geometric similarity as described by (11) requires that all dependence of $\tilde{\mathscr{P}}$ on y^+ be incorporated in f. Combining these two requirements, the fact that A is independent of y^+ means that it must be independent of k_{tot}^+ as well. That is, A may depend only on α in the central range of wave-numbers. While figures 8, 9 and 11 show that this prediction is not strictly upheld, yet neither is it at gross variance with the data. A qualitative explanation of the discrepancy can be made on the basis that the sublayer waves are the strongest at $\alpha \cong \frac{1}{4}$ while the largest waves are strongest at $\alpha \cong \frac{1}{10}$. The intermediate distribution of A provides a smooth transition between these limits and cannot therefore be completely independent of k_{tot}^+. However, we may also conjecture that at much higher Reynolds numbers than those tested here the gradient of A in k_{tot}^+ at constant α will be negligibly small.

The A distributions for the three Reynolds numbers may be described as more or less uniform in k between the two limits established by viscosity at the high k and tube dimension at the low k end. The extent of the distribution in ω at any k_z between these limits is roughly independent of k_z, spanning a range of about 10:1 in ω. If Reynolds number is decreased steadily, the two k limits may be projected to approach each other. Roughly,

$$\frac{(k_z^+)_{\max}}{(k_z^+)_{\min}} = \frac{0{\cdot}04}{2\nu/aU_\tau},$$

leading to the conclusion that no waves will exist for $aU_\tau/\nu < 50$. This corresponds to $R < 900$ which is in good agreement with the accepted lower limit for turbulent

tube flow. An interesting conclusion which can be drawn from this view of the structure 'shrinking' down to a pure sublayer form as R is decreased, is that the waves of sublayer size must be able to sustain themselves without the infusion of energy from any larger waves in the flow.

One implication of uniform distribution of A between the k_z limits is that the u velocity fluctuations observed in the sublayer, say at $y^+ = 10$, will move progressively to smaller average k_z^+ as R is increased. Compare, for example, figures 7 (n) and 7 (i) and observe how the lower k_z^+ are in much greater evidence at the high Reynolds number. The effect is quite gradual since the influence of very large waves is reduced according to the observed behaviour of the wave intensity function, f, at the low $k_{\text{tot}}^+ y^+$ end. Nevertheless, the relative intensity of the small sublayer waves should continue to diminish (roughly as $R^{-\frac{1}{2}}$). Assuming this prognosis is indeed borne out by subsequent data at much higher R, it is curious that the mean velocity profile in the sublayer–buffer layer region should remain unchanged as the characteristic size of the local wave structure increases.

6. Conclusion

When this experimental study was embarked upon, the existence of periodic transverse structure in the sublayer was known from visual evidence (Runstadler, Kline & Reynolds 1963), and the initial work was directed toward confirming this with hot-wire measurement. Since visualization methods gave little evidence of transverse periodicity in larger sizes, we proceeded through the present study with an innate bias that the smallest waves which lie wholly in the sublayer and buffer layer were somehow different from the larger waves which involve the log layer. Therefore, it was with considerable surprise that we discovered a simple intensity correction procedure (§ 3) which brings sublayer waves (which must have strong viscid effects) into the family of log layer waves. While this result simplifies the task of reporting the data, it is not easy to understand why it happens.

One major limitation in this work is imposed by the absence of correlations with $y_1 \neq y_2$. The reader is cautioned not to interpret the wave intensity function f too literally as the y distribution of $\hat{u}$. As discussed in the appendix, it is not likely that all waves of a given size, k_{tot}, will have precisely the same $\hat{u}(y)$, so the measured f must be interpreted as an ensemble average of the intensity distributions of all the actual waves. To obtain a measure of the 'spread' of the distributions about the average requires the detailed data given by radial correlations. Of course these correlations contain much more information than just intensity, and will give the relative phase of the velocity components at different y as well (i.e. the full complex functions h_1 and h_2 introduced in the appendix).

While the component u is by far the easiest to measure, it is unfortunate that it is a combination of the natural wave components $\hat{u}$ and $\hat{w}$. Only the component v remains invariant with wave angle, and therefore is the only one which can be used by itself to test the similarity hypothesis over a large angle range. However, it is very difficult to measure v close to a surface, so it may be necessary to resort to u and w at low y^+. This is especially unpleasant, since three correlations,

uu, ww and uw, must all be measured. Thus, while the similarity hypothesis points ultimately to a very compact complete description of turbulence in tubes, it is certain that much additional careful work will be required before all the details have been nailed down. The success of the similarity hypothesis also gives hope that the mechanism of wave interactions, by which this entire equilibrium structure is sustained, can be described in equally concise terms.

We will close with a remark about the implications of the present results to theoretical analysis of turbulent tube flow. The only logical interpretation of the data is that dominant turbulence energy found at any station in the flow is in structures which extend all the way from that station to the surface. Thus, for equilibrium turbulent flows of this kind, and equilibrium boundary layers must be included in that definition, analysis which is concerned with disturbances small compared with the distance from the surface is dealing, at best, with a very small part of the turbulence.

Appendix. Some analytic implications of geometric similarity

A wave of the kind pictured in figure 8 is two-dimensional since $\partial/\partial\hat{x} = 0$. Throughout this appendix we will use letter subscripts to indicate partial differentiation. The continuity equation for the turbulence components, v and $\hat{w}$,

$$v_y + \hat{w}_{\hat{z}} = 0 \tag{A 1}$$

leads to the stream function, $\psi(y,\hat{z})$ for which

$$v = -\psi_{\hat{z}}, \quad \hat{w} = \psi_y. \tag{A 2}$$

The Navier–Stokes equations are then

$$\nabla^2\psi_t + v(\nabla^2\psi_y + U_{yy}\sin\alpha) + (\hat{w} + U\sin\alpha)\nabla^2\psi_{\hat{z}} = \nu\nabla^4\psi, \tag{A 3}$$

$$\hat{u}_t + v(\hat{u}_y + U_y\cos\alpha) + (\hat{w} + U\sin\alpha)\hat{u}_{\hat{z}} = \nu\nabla^2\hat{u}, \tag{A 4}$$

where ∇^2 is simply $(\partial^2/\partial y^2) + (\partial^2/\partial\hat{z}^2)$. Geometrically similar wave solutions can be written in the form

$$k\psi = b_1(\alpha)\,h_1(ky)\exp\{jk(\hat{z} - Ct)\}, \tag{A 5}$$

$$\hat{u} = b_2(\alpha)\,h_2(ky)\exp\{jk(\hat{z} - Ct)\}, \tag{A 6}$$

where h_1 and h_2 are complex functions. The appropriate mean velocity distribution is

$$U = B_1 + B_2\log y. \tag{A 7}$$

Substitution of these three into the Navier–Stokes equations yields

$$\left\{\left[\left(U - \frac{C}{\sin\alpha}\right)b_1(h_1'' - h_1) - \frac{B_2 b_1 h_1}{(ky)^2}\right]\sin\alpha - \frac{\nu k b_1(h_1^{iv} - 2h_1'' + h_1)}{j}\right\}\exp\{jk(z - Ct)\}$$
$$= \text{non-linear terms}, \tag{A 8}$$

$$\left\{\left(U - \frac{C}{\sin\alpha}\right)b_2 h_2\sin\alpha + \frac{B_2 b_1 h_1}{ky}\cos\alpha - \frac{\nu k b_2(h_2'' - h_2)}{j}\right\}\exp\{jk(z - Ct)\}$$
$$= \text{non-linear terms}, \tag{A 9}$$

where the superscript primes indicate differentiation. If the non-linear terms are ignored, the first of these is the familiar Orr–Sommerfeld equation with a special choice of average velocity profile. At Reynolds numbers of interest here, the viscid terms are very small, yet in a purely linear theory they must be retained at the critical layer where $U \cong C/\sin\alpha$, and in the sublayer where $y \cong 0$. In fully developed turbulent flow it is the non-linear terms which assume importance at the critical layer. Viscous influences are significant only in the sublayer, and for present purposes may be neglected. The brief analysis here is not complete enough to handle correctly the wave interactions which figure in a non-linear theory so this will not be attempted.

Consider then the linear inviscid terms in (A 8). In order that these be independent of absolute scale, k, it is necessary that $U - C/\sin\alpha$ be a function of ky only. This is equivalent to the condition

$$\frac{C}{\sin\alpha} = B_1 - B_2 \log mk, \tag{A 10}$$

where m is an arbitrary constant. Comparison with (A 7) shows that

$$\frac{C}{\sin\alpha} = U(y_0), \tag{A 11}$$

where

$$y_0 k = 1/m. \tag{A 12}$$

The wave speed is seen to match the mean velocity component (projected into the wave cross-section) at a distance from the surface inverse to k. That is, the location of the critical layer is geometrically scaled.

Consider next the linear inviscid terms in (A 9). In order that these terms be independent of α it is necessary that

$$b_2/b_1 = \cot\alpha. \tag{A 13}$$

Thus we anticipate that waves with small inclination should have $\hat{u}$ much stronger than v or $\hat{w}$, while the reverse should be true for waves with large α. This behaviour is confirmed by surface pressure fluctuation data. Since surface pressure is related to the v and $\hat{w}$ components (by integration of the y momentum equation) the fact that surface pressure correlations are dominated by waves of large α† means that the same must be true of v and $\hat{w}$. By contrast, the longitudinal turbulence velocity is dominated by waves of small α.

The longitudinal turbulence component which constitutes the data of this paper is

$$u = \hat{u}\cos\alpha + \hat{w}\sin\alpha, \tag{A 14}$$

which may be squared to give

$$u^2 = \hat{u}^2\cos^2\alpha + \hat{u}\hat{w}\cos\alpha\sin\alpha + \hat{w}^2\sin^2\alpha. \tag{A 15}$$

† The first data of this kind was given by Willmarth & Wooldridge (1962). A more complete picture is given by Bull (1963).

From (A 2), (A 5), (A 6) and (A 14) the time-average part of the quadratic functions are

$$\hat{u}^2 = \tfrac{1}{2}h_2 h_2^* b_2^2,$$
$$\hat{u}\hat{w} = \tfrac{1}{4}(h_2 h_1'^* + h_2^* h_1') b_1 b_2, \tag{A 16}$$
$$\hat{w}^2 = \tfrac{1}{2}h_1' h_1'^* b_1^2,$$

where the superscript * denotes complex conjugate. Now if h_2 were to be a precisely determined function then $h_2 h_2^*$ would be exactly a scalar multiple of $f(ky)$ given in figure 9. More likely, waves of a given k are associated with a distribution of functions, h_2. Then $f(ky)$ must be regarded as an ensemble average of this distribution and the statement of geometric similarity is extended to the ensemble. Taking ensemble averages (with respect to h_1 and h_2) of (A 16) we have

$$E_h[\hat{u}^2] = f(ky) b_2^2,$$
$$E_h[\hat{u}\hat{w}] = g_1(ky) b_1 b_2, \tag{A 17}$$
$$E_h[\hat{w}^2] = g_2(ky) b_1^2,$$

where

$$g_1 = E_h[\tfrac{1}{4}(h_2 h_1'^* + h_2^* h_1')], \tag{A 18}$$
$$g_2 = E_h[\tfrac{1}{2}h_1' h_1'^*],$$

are both functions which have not yet been experimentally measured. An ensemble average of (A 15) can also be taken and then simplified with the aid of (A 13) and (A 18) to

$$E_h[u^2] = b_2^2(f\cos^4\alpha + g_1\cos^2\alpha\sin^2\alpha + g_2\sin^4\alpha)/\cos^2\alpha. \tag{A 19}$$

This function enclosed in parenthesis shows how the composition of $E[u^2]$ changes from f to g_1 to g_2 as α increases from 0 to $\frac{1}{2}\pi$.

REFERENCES

Bradshaw, P. 1967 Inactive motion and pressure fluctuation in turbulent boundary layers. *J. Fluid Mech.* **30**, 241.

Bull, M. K. 1963 Properties of the fluctuating wall-pressure field of a turbulent boundary layer. *AGARS Report*, no. 455.

Clark, J. A. 1968 A study of incompressible turbulent boundary layers in channel flow. *Am. Soc. Mech. Engng Paper* 68-FE-26 (*J. Basic Eng.*).

Favre, A. J., Gaviglio, J. J. & Dumas, R. J. 1958 Further space–time correlations of velocity in a turbulent boundary layer. *J. Fluid Mech.* **3**, 344.

Grant, H. L. 1958 The large eddies of turbulent motion. *J. Fluid Mech.* **4**, 149.

Landahl, M. T. 1967 A wave-guide model for turbulent shear flow. *J. Fluid Mech.* **29**, 441.

Laufer, J. 1953 The structure of turbulence in fully developed pipe flow. *NACA* TN 2954. Also Rep. no. 1174 (1954).

Lin, C. C. 1955 *The Theory of Hydrodynamic Stability*. Cambridge University Press.

Lumley, J. L. 1967 *Proceeding of the International Colloquium on the Fine Scale Structure of the Atmosphere and its Influence on Radio Wave Propagation*. Moscow: Doklady Adademia Nauk, SSSR.

Morrison, W. R. B. 1969 Two-dimensional frequency—wave-number spectra and narrow band shear stress correlations in turbulent pipe flow. Ph.D. thesis, University of Queensland, Brisbane, Australia.

Runstadler, P. W., Kline, S. J. & Reynolds, W. C. 1963 An experimental investigation of the flow structure of the turbulent boundary layer. *Report MD 8 Thermoscience Div., Mech. Engr. Dept., Stanford University.*

Willmarth, W. W. & Wooldridge, C. E. 1962 Measurements of the fluctuating pressure at the wall beneath a thick turbulent boundary layer. *J. Fluid Mech.* **14**, 187.